arXiv:0908.4283v3 [astro-ph.SR] 28 Apr 2010

Draft for ApJ, April 29, 2010

Production of ^{26}Al, ^{44}Ti, and ^{60}Fe in Core-Collapse Supernovae: Sensitivity to the Rates of the Triple Alpha and ^{12}C$(\alpha,\gamma)^{16}$O Reactions

Clarisse Tur[1]

National Superconducting Cyclotron Laboratory,
Michigan State University, 1 Cyclotron Laboratory, East Lansing, MI 48824-1321
Joint Institute for Nuclear Astrophysics

`tur@nscl.msu.edu`

Alexander Heger[1]

School of Physics and Astronomy, University of Minnesota, Twin Cities, Minneapolis, MN 55455-0149;
Nuclear and Particle Physics, Astrophysics and Cosmology Group, T-2, MS B227, Los Alamos National Laboratory, Los Alamos, NM 87545

`alex@physics.umn.edu`

Sam M. Austin[1]

National Superconducting Cyclotron Laboratory,
Michigan State University, 1 Cyclotron Laboratory, East Lansing, MI 48824-1321
Joint Institute for Nuclear Astrophysics

`austin@nscl.msu.edu`

ABSTRACT

We have studied the sensitivity to variations in the the triple alpha and ^{12}C$(\alpha,\gamma)^{16}$O reaction rates of the production of ^{26}Al, ^{44}Ti, and ^{60}Fe in core-collapse supernovae. We used the KEPLER code to model the evolution of $15\,\mathrm{M}_\odot$, $20\,\mathrm{M}_\odot$, and $25\,\mathrm{M}_\odot$ stars to the onset of core collapse and simulated the ensuing

---

[1] Joint Institute for Nuclear Astrophysics

supernova explosion using a piston model for the explosion and an explosion energy of 1.2×10^{51} erg. Calculations were performed for the Anders and Grevesse (1989) and Lodders (2003) abundances. Over a range of twice the experimental uncertainty, σ, for each helium-burning rate the production of ^{26}Al, ^{60}Fe, and their ratio vary by factors of five or more. For some species, similar variations were observed for much smaller rate changes, $0.5\,\sigma$ or less. The production of ^{44}Ti was less sensitive to changes in the helium-burning rates. Production of all three isotopes depended on the solar abundance set used for the initial stellar composition.

Subject headings: *gamma-rays: general, nuclear reactions, nucleosynthesis, abundances, supernovae: general*

1. Introduction

Observations of gamma rays from radioactive nuclei, and, in particular, from ^{26}Al, ^{44}Ti, and ^{60}Fe, with halflives of 7.2×10^{5} yr, 60 yr, and 2.62×10^{6} yr (Rugel et al. 2009), respectively, provide information about the sites and nature of stellar nucleosynthesis that is difficult to obtain in other ways. For example, the spatial distribution of ^{26}Al inferred from observation of its gamma rays indicates that their most probable source is massive stars; a comparison with the observed intensity of ^{60}Fe, ^{26}Al, and ^{44}Ti gamma rays provides a stringent test of supernova models; a comparison of the observed intensity of the ^{26}Al gamma rays and the calculated production of ^{26}Al in core-collapse supernovae provides an estimate of the rate of supernovae in the galaxy; the failure to observe ^{44}Ti gamma rays, other than from Cas A may indicate that emission of ^{44}Ti in supernovae is fairly rare, or that the supernova rate has been overestimated. For a discussion of these issues see Leising & Diehl (2009); Diehl et al. (2006a).

Observations have now yielded accurate gamma ray intensities for these nuclei (Diehl et al. 2006a and the references therein; Wang et al. 2007), but the reliability of deductions based on these intensities is limited by our understanding of the production mechanisms that synthesize ^{26}Al, ^{44}Ti, and ^{60}Fe. For example, estimates of the ratio ^{60}Fe/^{26}Al have varied greatly as discussed by Limongi & Chieffi (2006); Woosley & Heger (2007). Early calculations by Timmes et al. (1995) are in reasonable agreement with present results, whereas some later calculations using the same supernova code yield much different results. A detailed discussion, tracing these changes to the effects of reaction rate choices, can be found in Woosley & Heger (2007). Additional uncertainties arising from different astrophysical model assumptions or approximations are discussed in Woosley & Heger (2007); Limongi & Chieffi

(2006); Young & Fryer (2007). In addition, it appears that yields may be significantly different when simulations are done in two or three dimensions (Meakin & Arnett 2006).

The yield uncertainties resulting from reaction rate uncertainties that have been examined previously are mostly for reactions directly involved in the nucleosynthesis processes, but other reaction rate uncertainties may also be important. In their recent study of ^{26}Al and ^{60}Fe yields from massive stars Limongi & Chieffi (2006) showed that the amount of C fuel left by the standard helium burning affects all subsequent shell burning episodes and the yields of ^{26}Al and ^{60}Fe. Since the yields of ^{12}C and ^{16}O at the completion of core helium burning are determined by the rates for the triple-alpha ($R_{3\alpha}$) and $^{12}\mathrm{C}(\alpha,\gamma)^{16}\mathrm{O}$ ($R_{\alpha,12}$) reactions, we expect the yields of ^{26}Al and ^{60}Fe to depend on these rates. We have previously shown that the production factors for many isotopes with $A < 90$ depend strongly on both $R_{3\alpha}$ and $R_{\alpha,12}$ (Tur et al. 2007, 2009).

There have been several studies of the effects of uncertainties in these helium burning rates. Only a few have involved changes in $R_{3\alpha}$, mostly for studies of the effects of changes in coupling constants over long time scales. For example, Schattl, et al. (2004) investigated the effects of changes in the excitation energy of the Hoyle state at 7.65 MeV in ^{12}C but considered only large changes in rate and did not give yields for ^{60}Fe, ^{26}Al, and ^{44}Ti. Other authors have discussed the results of changes in $R_{\alpha,12}$ but yields of ^{60}Fe, ^{26}Al, and ^{44}Ti are not often given. Imbriani, et al. (2001) evolved a $25\,\mathrm{M}_\odot$ star at two values of $R_{\alpha,12}$ which differ by a ratio of 2.35, corresponding to about 0.7 and 1.6 on the rate scales we use for $R_{\alpha,12}$ if one normalizes to the value of the rate at 300 keV. We will show a comparison with the Imbriani, et al. results in Section 3. Hoffman, et al. (1999) used two different $R_{\alpha,12}$ and present results for a $15\,\mathrm{M}_\odot$ star, but also changed many other reaction rates so an accurate comparison with our results is not possible.

It is clear that available studies do not provide a detailed estimate of the variation of the yields of ^{60}Fe, ^{26}Al, and ^{44}Ti with changes in the helium burning rates. This shortcoming is especially important because one anticipates that the variation of the yields with rates might be rapid. The lifetimes of the long lived isotopes depend strongly on the temperature of their environment. For example, Limongi & Chieffi (2006), note that the lifetime of ^{26}Al drops to 0.19 yr at $\log(T/\mathrm{K}) = 8.4$ and that of ^{60}Fe to 0.5 yr at $\log(T/\mathrm{K}) = 9$. Their yields will then depend on whether or not they are formed in a convective region of the star and are carried relatively quickly to cooler regions. Since the details of the convective structure of a star depend on the helium burning rates, we expect that the production of ^{60}Fe, ^{26}Al, and ^{44}Ti might show a similar sensitivity. A detailed study, with closely spaced rate changes is necessary.

In this paper we describe a systematic study of the changes in supernovae synthesis of ^{26}Al, ^{44}Ti, and ^{60}Fe that result from changes in the helium burning reaction rates and changes in the initial stellar abundances. The emphasis is not on the *absolute* yields, but on the *variations* in the yields induced by changes in the helium burning reaction rates and the initial abundances. In total about 200 stars were evolved; the specific values of the helium burning rates used are shown in Fig. 1 of Tur et al. (2007). We find that over the $\pm 2\sigma$ range of rates, the yield changes are large, often a factor of five or more, and that the yields of ^{60}Fe, and ^{26}Al often vary rapidly with reaction rate and do not show simple monotonic behavior.

In §2 we present details of the calculations. In §3, we compare our results for the standard values of the helium burning reaction rates to prior calculations (AG89 abundances), and then present the outcome of our rate and abundance changes for the three radioactivities under study. In §4, we discuss other important uncertainties that can impact the yield predictions and compare our results with results of observations. Our conclusions are given in §5.

2. Stellar models and reaction rates

We used the KEPLER code (Weaver et al. 1978; Woosley & Weaver 1995; Rauscher et al. 2002; Woosley et al. 2002) to simulate stellar evolution from standard hydrogen burning up to core-collapse; a piston placed at the base of the oxygen shell was then used to simulate the explosion. The outward velocity of the piston was set to impart a kinetic energy of 1.2×10^{51} erg to the ejecta as they escape to infinity. After estimating the fallback from the hydrodynamic supernova simulations, the final yields were determined by employing the parametrization of the mixing that was used by Woosley & Heger (2007). See Tur et al. (2007) for a more detailed description of the models.

We used the rates of Rauscher & Thielemann (2000) for the ^{26}Mg(p,n), ^{26}Al(n,p), ^{26}Al(n,α), ^{40}Ca(α,γ), ^{44}Ti(α,γ), ^{44}Ti(α,p), ^{59}Fe(n,γ), and ^{60}Fe(n,γ) reactions, the rates of Iliadis et al. (2001) for the ^{25}Mg(p,γ), and ^{26}Mg(p,γ) reactions, the rates of Fisker, et al. (2001) for the ^{44}Ti(α,p) reaction, and for ^{22}Ne(α,n) rate we used the lower limit from (Jaeger et al. 2001). The calculations described in this paper were performed over a significant time period. Sometimes the preferred rates changed over that period, but because of our desire for a systematic set of studies, focusing on the rates of the helium burning reactions, we retained our initial choices for the entire set of simulations. We expect that our simulations will provide a reasonable estimate of the *relative* yield uncertainties resulting from the uncertainties in the helium burning rates, even if other rates or approximations change. A good overview over the reaction rates used can also be found in Rauscher et al. (2002).

We calculated ^{26}Al, ^{44}Ti and ^{60}Fe yields for $\pm 2\,\sigma$ variations of $R_{3\alpha}$ and $R_{\alpha,12}$ from their standard values as given by Caughlan & Fowler (1988) and by 1.2 times the rate recommended by Buchmann (1996), respectively. The $\pm 1\,\sigma$ experimental uncertainties were taken to be 12 % and 25 %. We performed calculations for 15 $M_\odot$, 20 $M_\odot$, and 25 $M_\odot$ stars and for three different rate sets: (1) $R_{3\alpha}$ was kept constant at its value from Caughlan & Fowler (1988), and $R_{\alpha,12}$ was varied; (2) $R_{\alpha,12}$ was held constant at 1.2 times the rate recommended by Buchmann (1996) and $R_{3\alpha}$ was varied; (3) both standard values of the rates were varied by the same factor, so their ratio remained constant, to investigate the extent to which only the ratio of the two rates is important.

We also determined the yields for two different stellar compositions: Lodders (2003) and Anders & Grevesse (1989), hereafter L03 and AG89. The L03 abundances for C, N, O, Ne are rather close to those of Asplund, et al. (2009).

3. Results

3.1. Comparison with previous calculations

In Table 1, we show the final yields for ^{26}Al, ^{44}Ti, and ^{60}Fe for our 15 $M_\odot$, 20 $M_\odot$, and 25 $M_\odot$ stars, and their average using a Scalo (Scalo 1986) Initial Mass Function (IMF) with a slope of $\gamma = -2.6$, for the standard values of $R_{3\alpha}$ and $R_{\alpha,12}$, and for both the AG89 and the L03 abundances. The difference in the yields due to the initial composition is largest for the 25 $M_\odot$ star, where the yields are reduced by $\sim$ 28 %, $\sim$ 15 %, and $\sim$ 81 % for ^{26}Al, ^{44}Ti, and ^{60}Fe, respectively, in going from the AG89 to the L03 abundances. This effect is significant, but smaller than the effect of variations in the helium burning rates, as we shall see in the next subsection. The major difference in the abundance sets is the substantially reduced CNO content of L03 compared to AG89 (see Fig. 2 in Tur et al. 2007). The central carbon mass fraction for the 25 $M_\odot$ star, however, changes only by about 5 % and is 0.1903 (0.1790) for the AG89 (L03) abundances (Tur et al. 2007). The IMF-averaged values for ^{26}Al and ^{44}Ti are very similar for the two abundance sets.

Figure 1 shows a comparison of our results for the yields of ^{26}Al, ^{44}Ti, and ^{60}Fe (for standard values of $R_{3\alpha}$ and $R_{\alpha,12}$, and the AG89 abundances), and the results from some recent calculations: in Figure 1*a* our ^{26}Al yields are shown together with those of Limongi & Chieffi (2006); Rauscher et al. (2002); Thielemann et al. (1996); Timmes et al. (1995) (the latter is based on the survey by Woosley & Weaver 1995); in Figure 1*b*, we compare our ^{60}Fe yields to those of Limongi & Chieffi (2006); Rauscher et al. (2002); Timmes et al. (1995); in Figure 1*c*, the ^{44}Ti yields are plotted for our study as well as for Rauscher et al. (2002);

Thielemann et al. (1996). The Thielemann et al. (1996) yields for ^{60}Fe are not shown because they were much smaller than the yields shown here. Limongi & Chieffi (2006); Timmes et al. (1995) only studied the yields for ^{26}Al and ^{60}Fe, so no ^{44}Ti yield can be shown.

The ^{26}Al yields found for most of these studies are in rough agreement, given the uncertainties due to reaction rate choices and astrophysical model differences described in the Introduction. The larger differences for ^{60}Fe can mainly be explained by the reaction rate differences discussed in Woosley & Heger (2007). The yield curves of Figure 1 for the present study have dips at $20\,\mathrm{M}_\odot$ for the three isotopes studied in this paper. This dip corresponds to an inversion of the monotonically increasing general trend in the mass-radius relation as noted by Limongi & Chieffi (2006). A related behavior for the $20\,\mathrm{M}_\odot$ star was observed for medium-weight isotopes (Tur et al. 2007; Rauscher et al. 2002), as a result of merging of the O, Ne, and C burning shells about a day prior to the supernova explosion.

3.2. Effect of variations of the helium burning reaction rates

We adopt a three-character notation to label our plots, e.g., LA3, similar to the notation adopted by Tur et al. (2007). The first character can be an "L" (to denote the L03 initial abundances) or an "A" (for the AG89 initial abundances). The second character denotes the study: "A", when $R_{3\alpha}$ was kept constant, and $R_{\alpha,12}$ was varied, "B", when both rates were varied by the same factor, so their ratio remained constant, and "C", when $R_{\alpha,12}$ was held constant, and $R_{3\alpha}$ was varied. The third character is the number of stars included in the IMF average; it is typically 3, for averages over the three stars ($15\,\mathrm{M}_\odot$, $20\,\mathrm{M}_\odot$, and $25\,\mathrm{M}_\odot$). When no third character is present the values apply to a single star.

Figures 2*a*-*f* show the yields of ^{26}Al, ^{44}Ti, and ^{60}Fe for the $25\,\mathrm{M}_\odot$ star as a function of reaction rate for the three sets of rates (see Introduction) and for the two abundance sets we used: AG89 and L03. Figures 3*a*-*f* show the same for the IMF-averaged yields. The yield often varies non-monotonically and sharply with rate. We find a strong dependence of the yields on $R_{3\alpha}$ and $R_{\alpha,12}$, and a smaller dependence on the initial solar abundances. The strongest variations occur for the ^{60}Fe yields, with weaker variation for the ^{26}Al yields, and still weaker variations for ^{44}Ti.

For the L03 abundances, in the LA series for the $25\,\mathrm{M}_\odot$ star, the ^{60}Fe yield reaches a maximum value of $3.590\times10^{-4}\,\mathrm{M}_\odot$ when $R_{\alpha,12}$ is reduced by 24 % (relative to its standard value), and a minimum of $8.285\times10^{-6}\,\mathrm{M}_\odot$ when it is reduced by 48 %, a factor of ~ 43 change in yield. Changes in $R_{3\alpha}$ can cause similarly large effects: in the LC series for the $25\,\mathrm{M}_\odot$ star, the ^{60}Fe yield is at it maximum value of $2.400\times10^{-4}\,\mathrm{M}_\odot$ when $R_{3\alpha}$ is increased by 24 % (relative to its standard value), and a minimum value of $2.881 \times 10^{-5}\,\mathrm{M}_\odot$ when $R_{3\alpha}$ is reduced by 6 %, a factor of $\sim$ 12 change. Even for ^{44}Ti, differences of a factor of about 2 are observed for certain cases. The differences for the IMF averaged case are somewhat smaller but still substantial, especially for ^{60}Fe.

For the AB and LB series, where both rates are a given multiple of their standard values, the variations are weaker. The variation of the central carbon abundances with reaction rate is about one-third of that for comparable variation of the reaction rate $R_{\alpha,12}$ alone (Tur et al. (2007)). This is consistent with the generally weaker variations in the yields of the radioactive nuclides.

Since the half-lives of ^{26}Al and ^{60}Fe ($\sim 10^6$ yr) are much longer than the average time between two galactic SNII events ($\sim$ 2 per century), a steady state assumption, where the production rate balances the decay rate is reasonable. The changes in the production yields discussed above then translate directly into changes in the predicted photon flux.

More detailed results for variation of $R_{3\alpha}$ and $R_{\alpha,12}$, and for the two initial abundance sets are given in Tables 2 and 3.

We can compare our results to those of Imbriani, et al. (2001) at $R_{\alpha,12} = 0.7$ and 1.6. Since we did not do simulations at these exact values, we have read values from Fig. 2*a*. The results, especially for ^{60}Fe, are subject to large extrapolation uncertainties. The energy dependencies of the reaction rates also differ. The ratio of our results at 0.7 to those at 1.6 for ^{26}Al (^{60}Fe) is 0.8 (0.6) and those of Imbriani, et al. is 0.17 (1.22). Individual values of the yields agree within a factor of $2-3$. It is difficult to judge whether these differences are significant, given the different assumptions on stellar physics that entered the calculations, as outlined in the introduction.

3.3. Production mechanisms

Figure 4 shows the yields of ^{26}Al, ^{44}Ti, and ^{60}Fe for a $25\,\mathrm{M}_\odot$ star using the L03 abundances at various stages of stellar evolution for the standard values of $R_{3\alpha}$ and $R_{\alpha,12}$ (Figure 4*a*) and when $R_{3\alpha}$ is increased by 18 %, $R_{\alpha,12}$ maintained at its standard value (Figure 4*b*). The stellar burning stages for which yields are plotted and that are also used in Figure 5 are:

He-ign: At this time 1 % of the helium has burnt in the center.

He-dep: Just before central He depletion (when the central He mass fraction has reached 1 %).

C-ign: Just before central C ignition (when the central temperature reaches a value of 5×10^8 K). Central helium burning has finished.

C-dep: Central C depletion (when the central temperature has reached 1.2×10^9 K). Central C burning contributes mostly to those regions of the star below the mass cut.

O-dep: At central O depletion (when the central O mass fraction has dropped below 5 %).

Si-dep: Central Si depletion (when the central Si mass fraction drops below 10^{-4}).

pre-SN: At the pre-supernova stage when the contraction speed in the iron core reaches $1000\,\mathrm{km\,s^{-1}}$. This is typically about 0.25 s before core bounce.

SN unmix: 100 s after the passage of the shock wave. At this time all thermonuclear reactions and neutrino-process have essentially ceased, but Rayleigh-Taylor (RT) instabilities that cause mixing after the passage of the shock have not yet mixed the ejecta (in our approximation). This is only shown in Figures 5*d*, 5*e*.

Final: > 100 s after the passage of the shock wave. This includes mixing due to RT instabilities parametrized as in (Rauscher et al. 2002) and fallback (see also Young & Fryer 2007). In Figures 5*e,f* this has been labeled as "*SN mix*".

The convective history for the above two cases is shown in Figure 5*a,b* and the times of the snap-shots are indicated. Figure 5*c,d* shows the pre-supernova structure for these two cases including convective regions and mass fractions of ^{26}Al, ^{44}Ti, and ^{60}Fe. The inner dark gray region indicates iron core where we no longer follow detailed nucleosynthesis as these regions become part of the collapsing iron core and disappear in the remnant. Figure 5*e,f* shows the distribution of the isotopes inside the star at the different evolution stages. Here, light gray regions indicate where detailed nucleosynthesis was no longer followed. Notably, in both of the last two rows of Figure 5 the vertical solid black line indicates the location of the "mass cut" after the supernova explosion - everything below that line disappears in the remnant. The solid lines and symbols in Figure 4 show only the contributions outside the this mass cut, the dashed line and hollow symbols show mass contained in the entire star as computed at each stage. In general, the piston in the SN explosion can be below the mass cut if there is "fallback" – mass that has first moved outward during the SN explosion, but then did not escape and fell back onto the compact remnant instead; in the specific cases shown here there was not such "fallback".

As is shown in Figure 5*a,b* changes in reaction rates can cause significant differences in the convective history of a star. Convective zones can carry radioactive nuclei to cooler zones of the star where their effective lifetime is longer and their survival is enhanced. It can bring nuclei to hot regions where they can be destroyed, or transport "fuel" to very hot regions to synthesize nuclei. In our case we find a convective oxygen-burning shell visible at roughly $2\,\mathrm{M}_\odot$. In Figure 5*a*, this shell starts at approximately log(time till core collapse / yr)[1] of -3 and mixes with the carbon-rich layer above, whereas in Figure 5*b* where $R_{3\alpha}$ is increased by 18 % this burning layer starts at log(time till core collapse / yr) of -3.5 but does not mix with the carbon-rich layer above. In the case of merged layers ^{60}Fe is efficiently destroyed whereas it remains unchanged in the separated carbon layer (Figures 5*c* and 5*d*). ^{44}Ti, on the other hand, is efficiently produced at the bottom of the hot merged layer and mixed out throughout the entire convective domain, whereas in the case of separated layers only some of it is made at the bottom of the oxygen-burning layer and little is made in the carbon layer. The merging of the layers is also not beneficial to the production of ^{26}Al; this works better at the bottom of the separated carbon-burning layer of the star with the increased $R_{3\alpha}$.

3.4. ^{26}Al

A substantial amount of ^{26}Al is already present at core helium ignition as a result of the $^{25}\mathrm{Mg}(\mathrm{p},\gamma)^{26}\mathrm{Al}$ reaction occurring during core H burning. This reaction is essentially the only means of production of ^{26}Al, even during the later stages of stellar evolution. During core helium burning we see most of ^{26}Al in the H envelope with an abundance peak at the location of the hydrogen-burning shell. In the helium-burning core ^{26}Al is mostly destroyed. The amount of ^{26}Al remains essentially constant until core O depletion and then increases in the later stages of stellar evolution where ^{26}Al is made in C shell burning. The amount finally ejected after explosion is about an order of magnitude larger than the amount present at helium ignition. A discussion of the reactions that create and destroy ^{26}Al in later burning stages is given in Limongi & Chieffi (2006).

3.5. ^{60}Fe

Only a negligible amount of ^{60}Fe ($\sim 3\times10^{-15}\,\mathrm{M}_\odot$) is present at core helium ignition. That amount rapidly increases to $\sim 1\times10^{-7}\,\mathrm{M}_\odot$ at core helium depletion and gradually builds up through the later stages until explosion. Most of it is found at the lower part of the split He-burning shell and is made *after* central oxygen depletion. This last point underscores the importance of virtually every stage in the star's life for the production of this isotope. ^{60}Fe is mainly produced by neutron capture on ^{59}Fe and destroyed by ^{60}Ni(n,γ)reactions. When the standard values of the helium burning rates are used, the pre-SN results show the destruction of some ^{60}Fe; when $R_{3\alpha}$ is increased by 18 %, this does not occur. This is due to the merging of the oxygen-burning and carbon-burning layers in the standard case which is not present in the case with the increased $R_{3\alpha}$ (Figure 5). ^{60}Fe from the entire carbon-rich convective zone can be mixed to the bottom of the very hot oxygen layer where it is partially destroyed. The ^{60}Fe present in the He shell is not directly affected by this destruction, but due to the merging layers, the shell gets less hot and hence produces less ^{60}Fe (Figure 5*e,f*). There is a significant difference between the amount of ^{60}Fe ejected in those two cases: $3.933\times10^{-5}\,M_\odot$ and $2.201\times10^{-4}\,M_\odot$, respectively, just as a result of variations in the helium burning rates.

---

[1] Here we assume that the core collapses in 250 ms after the end of our pre-SN calculation, when the iron core reaches an infall velocity of 1000 km/sec

3.6. ^{44}Ti

The amount of ^{44}Ti present at core helium ignition is minuscule - $\sim 0.25\,$g. It increases through the later burning stages, but remains below $1\times10^{-8}\,M_\odot$ outside of the mass cut until core Si depletion for the case $R_{3\alpha} = 1.18$, and still later for the standard values of the helium burning rates. ^{44}Ti is only made by O burning and later phases that all start off below the SN mass cut. A discussion of the reactions that create and destroy ^{44}Ti is given in Vockenhuber, C. et al. (2008). Remarkably, there is a significant amount of ^{44}Ti at the pre-SN stage just outside of the Fe-core in the Si-Shell. All of this disappears inside the remnant in these two cases; only some ^{44}Ti that is made in O shell burning is being ejected. This contribution is significantly bigger in the case of the merged O/Ne/C layers of the standard case as compared to the split layers of the case with $R_{3\alpha} = 1.18$. Whereas the standard case has 10x more ^{44}Ti in the pre-SN model outside the SN mass cut than the $R_{3\alpha} = 1.18$ case, the final production in both cases is entirely dominated by SN explosions. It would, therefore, be sensitive to uncertainties in the explosion energy and the asymmetries in the SN, and how these depend on a pre-SN structure, which is quite different in the two cases. That is, if the explosion was different in the two cases and not a "standard" 1.2×10^{51} erg explosion as we have assumed here, the ^{44}Ti yields might be quite different.

4. Discussion

We have shown that the uncertainties in the helium burning reaction rates cause large differences in the predicted yields of ^{26}Al, ^{44}Ti, and ^{60}Fe, with the changes in ^{60}Fe being particularly large. These yields are also sensitive to uncertainties in the rates of other important reactions and in the approximate treatment of convection (Limongi & Chieffi 2006; Woosley & Heger 2007); there may also be sites other than massive stars that contribute to the abundances of ^{26}Al, ^{44}Ti, and ^{60}Fe. The changes we have examined here, however, give a lower limit on the overall uncertainties which is sufficiently large so as to limit deductions that depend on their yields. Including other uncertainties will only make the situation worse.

We considered only stars with masses less than $30\,M_\odot$ and consequently did not include the contributions of Wolf-Rayet stars. In the models of Limongi & Chieffi (2006), Wolf-Rayet winds contribute less than half the yield of ^{26}Al in these heavier stars; Woosley & Heger (2007) find a similar contribution of wind and explosion for a $60\,M_\odot$ star. It seems reasonable to assume that the explosive process in Wolf-Rayet stars is subject to uncertainties similar to those we found for lighter stars, and that their overall contribution will be subject to similar uncertainties. This remains to be confirmed by further calculations.

Finally we consider two comparisons of the nucleosynthesis yields and astrophysical observations. As was mentioned above, in the steady state expected for isotope lifetimes short compared to galactic evolution times, the production rate of gamma rays is proportional to the amount of material made in a supernova explosion. Diehl et al. (2006b) have shown that the observed ^{26}Al gamma ray flux corresponds to a supernova rate of 1.9 ± 1.1 events/century for an assumed value of the supernova yield. Since the gamma ray flux is proportional to the supernova yield for ^{26}Al, it is subject to the uncertainties in the yield shown in Figure 3*a*-*f*; we must conclude that the uncertainty in this estimate of the supernova rate is much too small.

A second comparison is to the ratio of the gamma fluxes from ^{26}Al and ^{60}Fe. If one assumes that for both nuclei the gamma rays come from supernovae, and that the contributing supernovae have the same distribution in space, then the ratio of the fluxes is the ratio of the numbers of nuclei produced, or flux(60)/flux(26) = (26/60)(yield(60)/yield(26)). The yield ratios are shown in Figure 6*a*-*d*. These ratios should be compared to 60/26 times the flux ratios summarized in Table 2 of Wang et al. (2007), namely $(60/26)(0.15 \pm 0.06)$. The ratios shown in Fig. 6 are much larger for most values of the helium burning reaction rates, although the smallest values of the $^{12}\mathrm{C}(\alpha,\gamma)^{16}\mathrm{O}$ reaction rates do give ratios approaching the observed values. But given the size of the variations shown, it will not be possible to show that this value agrees with supernovae predictions until the helium burning reaction rates are much better known.

A different sort of comparison arises for ^{44}Ti. It is seen in the supernova remnant Cas A, but not elsewhere. Given conventional supernova rates, additional occurrences were expected (The et al. 2006). ^{44}Ti production is not particularly sensitive to the helium burning rates–see Figure 3*a*-*f*. Possible explanations include a lower production rate as occurs for some reaction rate combinations, or a lower supernova rate than assumed. As was pointed out above, ^{44}Ti production may be particularly sensitive to the supernova explosion physics. Young & Fryer (2007) have shown that these effects can be very large. A reference to our explosion model including supernova burning temperatures and time-scales as well as sensitivity of yields to explosion energy can be found in Woosley & Weaver (1995); Rauscher et al. (2002).

5. Conclusions

We explored changes in the core-collapse supernovae yields of ^{26}Al, ^{44}Ti, and ^{60}Fe arising from variations in the triple alpha and ^{12}C$(\alpha,\gamma)^{16}$O reaction rates. We find that these changes are significant, sometimes more than an order of magnitude from the minimum to the maximum yield within the $\pm 2\,\sigma$ range of rate uncertainty considered here for both reactions. The changes were most important for ^{60}Fe, smaller for ^{26}Al, and still smaller for ^{44}Ti. The yield-rate relationship was found to be complex, i.e., non-monotonic, and sometimes with large changes for small changes in reaction rates. For this reason it is difficult to give a simple statistical uncertainty for the effects of changes in a reaction rate. The high and low predictions provide a reasonable estimate for a given uncertainty range. For the triple alpha reaction $1\,\sigma$ rate changes are 1.0 ± 0.12 and for the ^{12}C$(\alpha,\gamma)^{16}$O reaction, 1.2 ± 0.3. Thus for a $25\,\mathrm{M}_\odot$ star, the ^{60}Fe yield varies by a factor of 5.0 (3.4) for $\pm 1\,\sigma$ variations of the triple alpha (^{12}C$(\alpha,\gamma)^{16}$O) rate. Other ranges can be determined from Tables 2 and 3. Obviously the detailed dependencies of the isotope production on the rates we varied may differ in other model calculations as they also depend on the stellar physics and modeling details.

We have isolated the effects on ^{26}Al, ^{44}Ti, and ^{60}Fe yields, of variations in the helium burning reaction rates within their experimental uncertainties. These effects turn out to be large and limit the conclusions we can draw from comparisons with observational data. They provide a lower limit to the total uncertainties that will remain even if all the uncertainties mentioned earlier are eliminated. This highlights the pressing need for improvements in our knowledge of the triple alpha and ^{12}C$(\alpha,\gamma)^{16}$O reaction rates.

We also explored the dependence of the ^{26}Al, ^{44}Ti, and ^{60}Fe yields on the initial solar abundances used for the initial composition of the star: Anders & Grevesse (1989) versus Lodders (2003). There again the dependence is complex, but smaller than that induced by changes in the helium burning reaction rates.

We thank Robert Hoffman for providing the solar abundance files used in this study and Stan Woosley for helpful discussions, including studies on the relative influence of the two reaction rates. This research was supported in part by the US National Science Foundation grants PHY06-06007 and PHY02-16783, the latter funding the Joint Institute for Nuclear Astrophysics (JINA), a National Science Foundation Physics Frontier Center. AH performed his contribution under the auspices of the National Nuclear Security Administration of the US Department of Energy at Los Alamos National Laboratory under contract DE-AC52-06NA25396, and has been supported by the DOE Program for Scientific Discovery through Advanced Computing (SciDAC; DE-FC02-01ER41176), and by the US Department of Energy under grant DE-FG02-87ER40328.

REFERENCES

Anders, E. & Grevesse, N. 1989, Geochim. Cosmochim. Acta, 53, 197

Asplund, M., Grevesse, G., Sauval, A. J. & Scott, P. 2009, ARA&A, 47, 481

Buchmann, L. R. 1996, ApJ, 468, L127; errata 1997 ApJ, 479, L153

Caughlan, G. R. & Fowler, W. A. 1988, At. Data & Nucl. Data Tab., 40, 283

Diehl, R., Prantzos, N. & von Ballmoos, P. 2006a, Nucl.Phys A, 777, 70

Diehl, R., Halloin, H. & Kretschmer, K. 2006b, Nature, 439, 45

Fisker, J. L., et al. 2001, ADNDT 79, 241

Hoffman. R. D., et al. 1999, ApJ, 521, 735

Iliadis, C., D'Auria, J. M., Starrfield, S., Thompson, W. J., & Wiescher, M. 2001, ApJS134, 151

Jaeger, M., Kunz, R., Mayer, A., Hammer, J. W., Staudt, G., Kratz, K. L., Pfeiffer, B. 2001, Phys. Rev. Lett., 87, 202501

Imbriani, G., et al. 2001, ApJ, 558, 903

Leising, M. & Diehl, R. 2009, arXiv:0903.0772v1 [astro-ph.HE]

Limongi, M. & Chieffi, A. 2006, ApJ, 647, 483

Lodders, K. 2003, ApJ, 591, 1220

Meakin, C. A. & Arnett, D. 2006 ApJ, 637, 53

Rauscher, T. & Thielemann, F.-K. 2000, ADNDT 75, 1

Rauscher, T., Heger, A., Hoffman, R. D., & Woosley, S. E. 2002, ApJ, 576, 323

Rugel. G., et al., 2009, Phys. Rev. Lett., 103, 072502

Scalo, J. M. 1986, Fund. Cosmic Phys., 11, 1

Schattl, H., et al. 2004, Ap&SS, 291, 27

The, L.-S., et al. 2006, A&A, 450, 1057

Thielemann, F.-K., Nomoto, K., & Hashimoto, M.-A. 1996, ApJ, 460, 408

Timmes, F. X., Woosley, S. E., Hartmann, D. H., Hoffman, R. D., Weaver, T. A., & Matteucci, F. 1995, ApJ, 449, 204

Tur, C., Heger, A., & Austin, S. M. 2007, ApJ, 671, 821

Tur, C., Heger, A., & Austin, S. M. 2009, ApJ, 702, 1068

Wang, W., et al., 2007 A&A, 469, 1005

Vockenhuber, C. et al. 2008, Journal of Physics G (Nuclear Physics), 35, 014034

Weaver, T. A., Zimmerman, G. B., & Woosley, S. E. 1978, ApJ, 225, 1021

Woosley, S. E. & Weaver, T. A. 1995, ApJ, 101, 181

Woosley, S. E., Heger, A., & Weaver, T. A. 2002, Rev. of Mod. Phys., 74, 1015

Woosley, S. E. & Heger, A., 2007, Phys. Rep. 442, 269

Young, P. A. & Fryer, C. L. 2007 ApJ, 664, 1033

This preprint was prepared with the AAS LaTeX macros v5.2.

Table 1. Yields $(M_\odot)\times10^5$: standard values of $R_{3\alpha}$ and $R_{\alpha,12}$.

	15 $M_\odot$	20 $M_\odot$	25 $M_\odot$	3 star ave.[a]
	AG89 abundances:			
^{26}Al	2.789	2.934	9.781	4.349
^{44}Ti	4.221	3.333	5.707	4.266
^{60}Fe	6.333	4.748	20.76	8.965
	L03 abundances:			
^{26}Al	2.443	5.962	7.023	4.535
^{44}Ti	4.263	4.039	4.846	4.322
^{60}Fe	7.481	1.727	3.933	4.924

[a] IMF-averaged over the 15, 20, and 25 $M_\odot$ models.

Table 2. Yields ($M_\odot$) for ^{26}Al, ^{44}Ti and ^{60}Fe as a function of the $R_{3\alpha}$ and $R_{\alpha,12}$ rates for stars of 15 $M_\odot$, 20 $M_\odot$, and 25 $M_\odot$ with AG89 initial abundances

	15 $M_\odot$			20 $M_\odot$			25 $M_\odot$			Three Star Average			
Rate Multiplier[a]	Al	Ti	Fe	Al	Ti	Fe	Al	Ti	Fe	Al	Ti	Fe	Fe/Al
$R_{3\alpha}$ varied, $R_{\alpha,12}$ constant													
(0.76,1.20)	2.31E-05	3.25E-05	4.32E-05	3.08E-05	3.92E-05	1.20E-04	4.17E-05	4.45E-05	6.79E-05	2.95E-05	3.72E-05	7.23E-05	2.45E+00
(0.82,1.20)	1.91E-05	3.68E-05	9.08E-05	3.89E-05	2.75E-05	8.98E-06	4.73E-05	3.79E-05	3.43E-05	3.13E-05	3.42E-05	5.35E-05	1.71E+00
(0.88,1.20)	2.45E-05	3.60E-05	5.32E-05	2.17E-05	3.27E-05	2.33E-05	8.45E-05	5.09E-05	5.39E-05	3.68E-05	3.82E-05	4.41E-05	1.20E+00
(0.94,1.20)	2.28E-05	4.03E-05	6.88E-05	4.30E-05	4.14E-05	1.64E-04	7.75E-05	5.70E-05	1.42E-04	4.10E-05	4.43E-05	1.14E-04	2.79E+00
(1.00,1.20)	2.79E-05	4.22E-05	6.33E-05	2.93E-05	3.33E-05	4.75E-05	9.78E-05	5.71E-05	2.08E-04	4.35E-05	4.27E-05	8.97E-05	2.06E+00
(1.06,1.20)	2.91E-05	4.26E-05	9.41E-05	2.54E-05	3.81E-05	1.27E-04	1.16E-04	5.86E-05	2.59E-04	4.67E-05	4.47E-05	1.40E-04	3.00E+00
(1.12,1.20)	2.35E-05	3.33E-05	1.23E-04	4.63E-05	6.24E-05	6.52E-05	7.89E-05	5.96E-05	2.68E-04	4.25E-05	4.79E-05	1.36E-04	3.21E+00
(1.18,1.20)	2.38E-05	3.30E-05	1.15E-04	4.02E-05	4.23E-05	5.36E-05	6.80E-05	4.96E-05	2.25E-04	3.84E-05	3.95E-05	1.20E-04	3.12E+00
(1.24,1.20)	2.24E-05	2.83E-05	1.94E-05	4.35E-05	4.09E-05	9.33E-05	5.53E-05	4.56E-05	1.85E-04	3.60E-05	3.59E-05	7.79E-05	2.17E+00
$R_{3\alpha}$ constant, $R_{\alpha,12}$ varied													
(1.000,0.624)	2.68E-05	3.77E-05	7.40E-06	3.30E-05	2.81E-05	1.33E-05	3.80E-05	3.11E-05	2.88E-05	3.12E-05	3.33E-05	1.39E-05	4.47E-01
(1.000,0.912)	2.81E-05	3.20E-05	7.39E-05	4.60E-05	3.90E-05	2.55E-05	5.56E-05	4.30E-05	1.63E-04	3.96E-05	3.65E-05	7.85E-05	1.98E+00
(1.000,1.056)	2.33E-05	3.22E-05	6.82E-05	4.41E-05	4.18E-05	4.88E-05	6.74E-05	4.96E-05	2.12E-04	3.92E-05	3.89E-05	9.33E-05	2.38E+00
(1.000,1.200)	2.79E-05	4.22E-05	6.33E-05	2.93E-05	3.33E-05	4.75E-05	9.78E-05	5.71E-05	2.08E-04	4.35E-05	4.27E-05	8.97E-05	2.06E+00
(1.000,1.344)	2.49E-05	3.64E-05	5.51E-05	4.08E-05	2.64E-05	8.09E-06	4.93E-05	4.30E-05	4.90E-05	3.52E-05	3.47E-05	3.92E-05	1.11E+00
(1.000,1.488)	2.43E-05	3.43E-05	5.08E-05	3.11E-05	3.95E-05	1.27E-04	4.27E-05	4.56E-05	4.87E-05	3.04E-05	3.84E-05	7.39E-05	2.43E+00
(1.000,1.776)	1.43E-05	4.19E-05	1.87E-04	2.65E-05	4.65E-05	1.40E-04	7.61E-05	6.37E-05	2.02E-04	3.13E-05	4.80E-05	1.76E-04	5.61E+00
(1.000,1.920)	1.42E-05	4.24E-05	1.72E-04	1.48E-05	4.60E-05	8.87E-05	5.51E-05	6.70E-05	1.72E-04	2.33E-05	4.89E-05	1.46E-04	6.29E+00

[a] The rate multipliers are given in the format ($R_{3\alpha}$ multiplier,$R_{\alpha,12}$ multiplier), where the rates being multiplied are the standard rate values chosen as described in the text

Table 3. Yields ($M_\odot$) for ^{26}Al, ^{44}Ti and ^{60}Fe as a function of the $R_{3\alpha}$ and $R_{\alpha,12}$ rates for stars of 15 $M_\odot$, 20 $M_\odot$, and 25 $M_\odot$ with L03 initial abundances

	15 $M_\odot$			20 $M_\odot$			25 $M_\odot$			Three Star Average			
Rate Multiplier[a]	Al	Ti	Fe	Al	Ti	Fe	Al	Ti	Fe	Al	Ti	Fe	Fe/Al
							$R_{3\alpha}$ varied, $R_{\alpha,12}$ constant						
(0.76,1.20)	1.44E-05	3.28E-05	3.97E-05	3.70E-05	5.00E-05	2.39E-04	8.620-05	5.74E-05	9.15E-05	3.71E-05	4.36E-05	1.12E-04	3.03E+00
(0.82,1.20)	1.30E-05	3.29E-05	1.00E-04	2.94E-05	4.22E-05	1.36E-04	6.81E-05	5.11E-05	6.27E-05	3.00E-05	3.97E-05	1.03E-04	3.44E+00
(0.88,1.20)	1.80E-05	3.60E-05	4.00E-05	2.83E-05	3.80E-05	7.28E-05	7.13E-05	4.97E-05	4.98E-05	3.26E-05	3.96E-05	5.22E-05	1.60E+00
(0.94,1.20)	1.90E-05	3.71E-05	4.00E-05	3.99E-05	5.10E-05	3.40E-05	6.88E-05	3.65E-05	2.88E-05	3.61E-05	4.12E-05	3.57E-05	9.89E-01
(1.00,1.20)	2.44E-05	4.26E-05	7.48E-05	5.96E-05	4.04E-05	1.73E-05	7.02E-05	4.85E-05	3.93E-05	4.54E-05	4.32E-05	4.92E-05	1.09E+00
(1.06,1.20)	2.45E-05	3.97E-05	8.71E-05	4.21E-05	4.04E-05	7.63E-05	8.64E-05	5.79E-05	1.51E-04	4.34E-05	4.39E-05	9.77E-05	2.25E+00
(1.12,1.20)	2.33E-05	3.73E-05	9.44E-05	2.54E-05	3.37E-05	5.34E-05	1.10E-04	5.81E-05	1.98E-04	4.27E-05	4.07E-05	1.04E-04	2.43E+00
(1.18,1.20)	2.14E-05	3.22E-05	3.11E-05	2.23E-05	3.89E-05	1.06E-05	1.27E-04	5.95E-05	2.20E-04	4.43E-05	4.01E-05	9.49E-05	2.14E+00
(1.24,1.20)	1.86E-05	2.86E-05	1.07E-05	4.15E-05	4.00E-05	4.43E-05	8.87E-05	6.08E-05	2.40E-04	4.06E-05	3.90E-05	7.02E-05	1.73E+00
							$R_{3\alpha}$ constant, $R_{\alpha,12}$ varied						
(1.000,0.624)	2.19E-05	2.74E-05	4.51E-06	3.15E-05	2.70E-05	1.22E-05	1.11E-04	4.91E-05	8.29E-06	4.45E-05	3.23E-05	7.71E-06	1.73E-01
(1.000,0.912)	2.72E-05	3.24E-05	3.87E-05	5.19E-05	4.10E-05	2.77E-05	1.10E-04	5.84E-05	3.59E-04	5.27E-05	4.07E-05	1.04E-04	1.98E+00
(1.000,1.056)	2.14E-05	3.22E-05	2.43E-05	2.24E-05	3.87E-05	9.25E-05	1.21E-04	5.94E-05	1.99E-04	4.31E-05	4.01E-05	8.30E-05	1.93E+00
(1.000,1.200)	2.44E-05	4.26E-05	7.48E-05	5.96E-05	4.04E-05	1.73E-05	7.02E-05	4.85E-05	3.93E-05	4.53E-05	4.32E-05	4.92E-05	1.09E+00
(1.000,1.344)	1.78E-05	3.62E-05	4.20E-05	2.82E-05	3.92E-05	8.94E-05	7.25E-05	5.19E-05	5.24E-05	3.28E-05	4.05E-05	5.87E-05	1.79E+00
(1.000,1.488)	1.32E-05	3.50E-05	3.86E-05	3.42E-05	4.72E-05	2.63E-04	7.61E-05	5.56E-05	1.02E-04	3.34E-05	4.33E-05	1.21E-04	3.63E+00
(1.000,1.776)	6.82E-06	3.52E-05	1.73E-05	1.29E-05	4.76E-05	9.11E-05	7.21E-05	6.92E-05	2.45E-04	2.27E-05	4.64E-05	8.85E-05	3.90E+00
(1.000,1.920)	1.14E-05	3.92E-05	1.92E-04	1.31E-05	4.86E-05	7.82E-05	3.65E-05	7.48E-05	2.44E-04	1.73E-05	4.98E-05	1.68E-04	9.72E+00

[a] The rate multipliers are given in the format ($R_{3\alpha}$ multiplier,$R_{\alpha,12}$ multiplier), where the rates being multiplied are the standard rate values chosen as described in the text

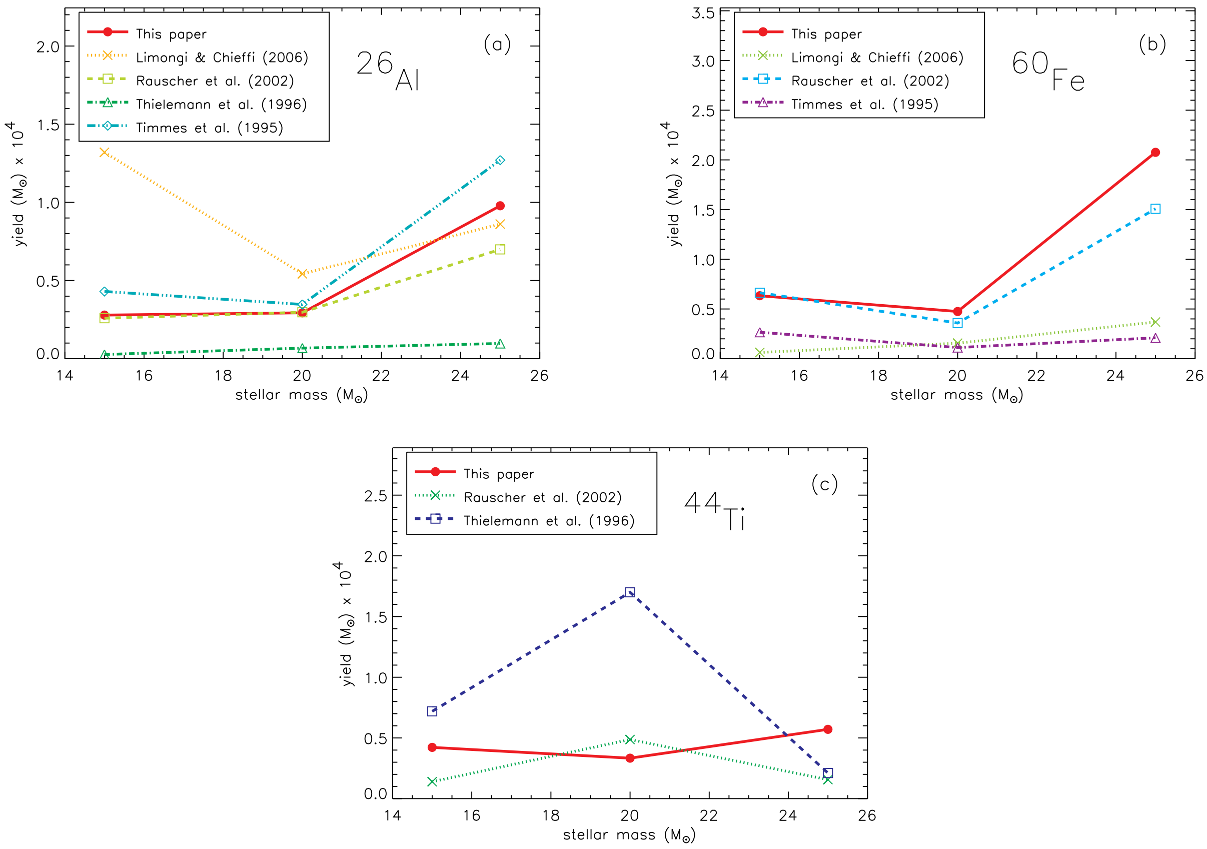

Fig. 1.— Yields versus stellar mass: comparison between the present study (standard values of the helium burning reaction rates, AG89 abundances) and previous publications. **(a)** ^{26}Al. **(b)** ^{60}Fe. **(c)** ^{44}Ti.

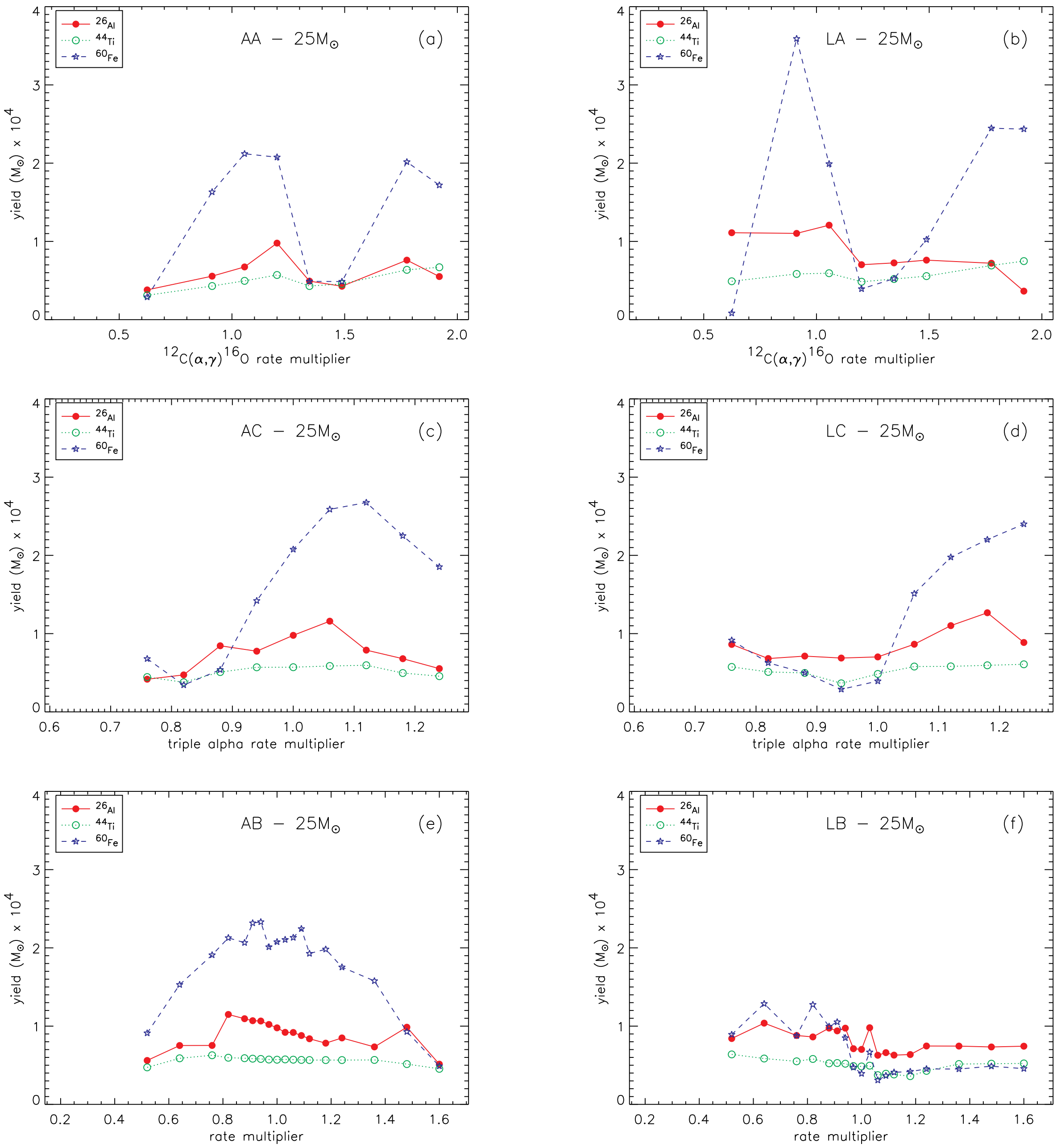

Fig. 2.— Yields versus reaction rate for the 25 $M_\odot$ model. For details see the text. **(a)** AA series. **(b)** LA series. **(c)** AC series. **(d)** LC series. **(e)** AB series. **(f)** LB series.

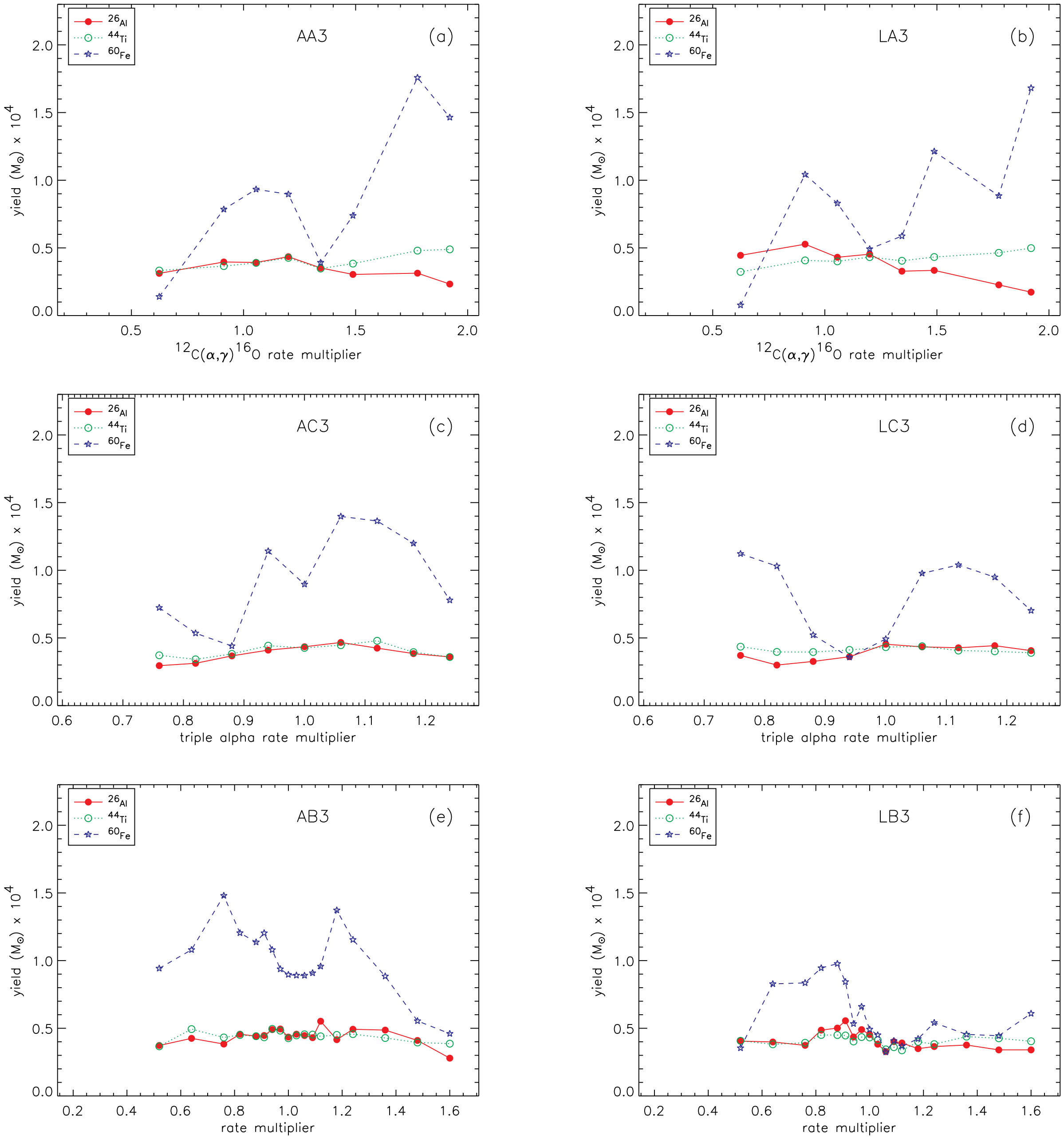

Fig. 3.— Yields versus reaction rate, averaged over 3 stars (15 M$_\odot$, 20 M$_\odot$, and 25 M$_\odot$). For details see the text. **(a)** AA series. **(b)** LA series. **(c)** AC series. **(d)** LC series. **(e)** AB series. **(f)** LB series.

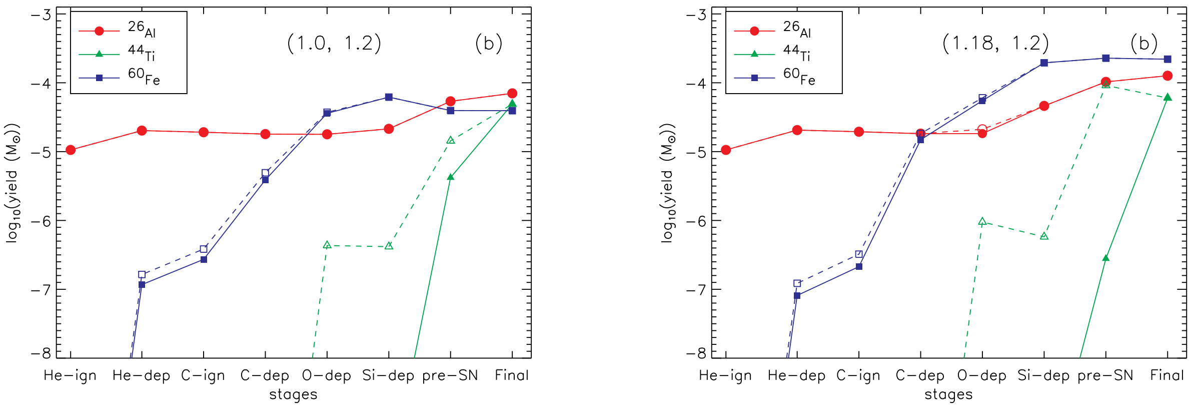

Fig. 4.— Solid symbols and lines give yields (total mass of the isotope outside the final mass cut of the SN, see Figure 5) at various evolutionary stages for a 25 M$_\odot$ star using the L03 initial abundances. The definition of the stages labeled on the abscissas are given in the text. The hollow symbols and lines show the total yield inside the star (including wind) as shown in the bottom row of Figure 5. **(a)** Standard values of the helium burning reaction rates (i.e., multipliers for $R_{3\alpha}$ and $R_{\alpha,12}$: 1.0 and 1.2, respectively). **(b)** $R_{3\alpha}$ higher by 18 % (i.e., multipliers for $R_{3\alpha}$ and $R_{\alpha,12}$: 1.18 and 1.2, respectively).

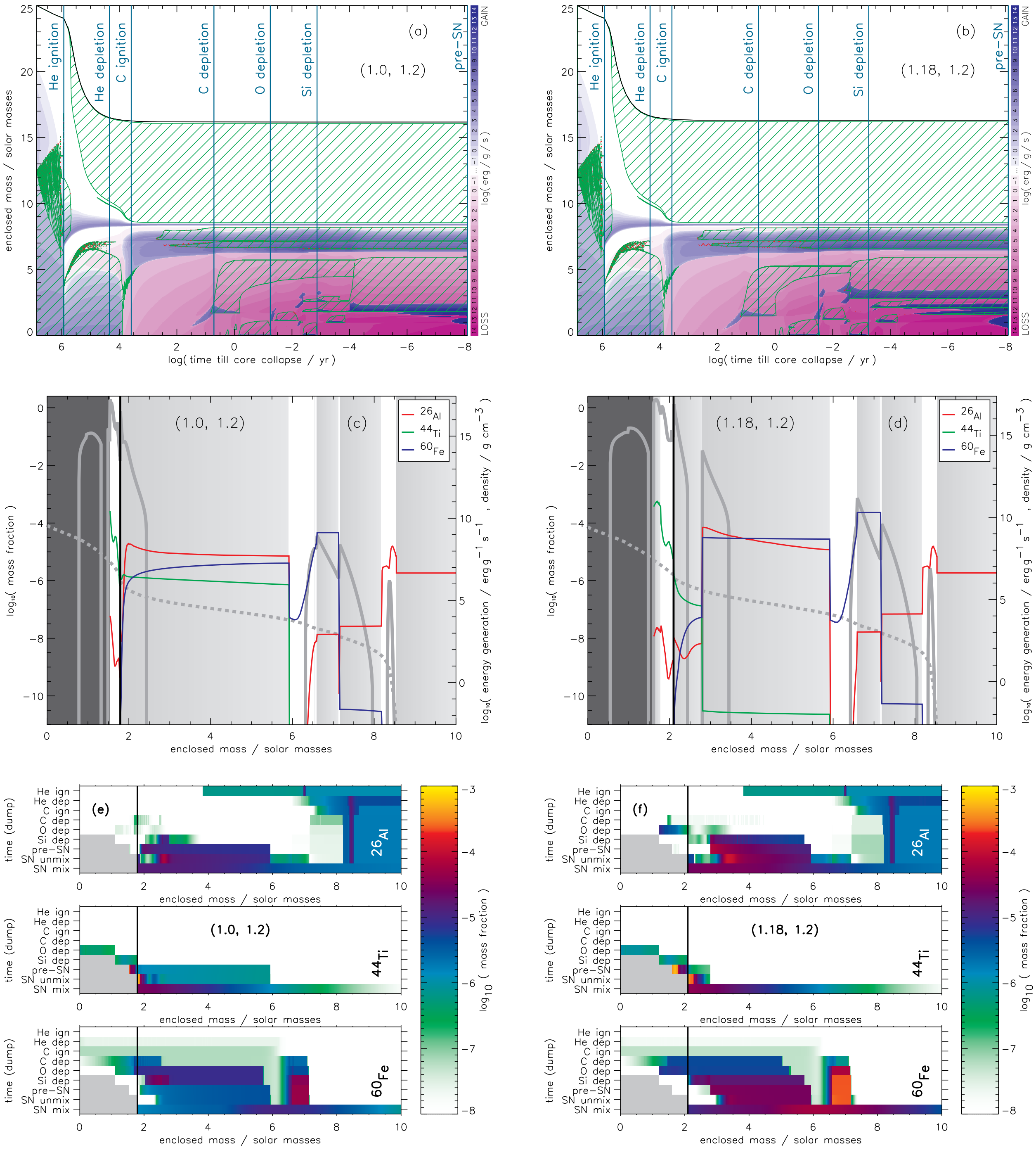
(a)
(1.0, 1.2)
(b)
(1.18, 1.2)
He ignition
He depletion
C ignition
C depletion
O depletion
Si depletion
pre−SN
enclosed mass / solar masses
log(time till core collapse / yr)
log(erg / g / s)
GAIN
LOSS
(c)
(d)
26Al
44Ti
60Fe
log₁₀(mass fraction)
log₁₀(energy generation / erg g⁻¹ s⁻¹ , density / g cm⁻³)
enclosed mass / solar masses
(e)
(f)
He ign
He dep
C ign
C dep
O dep
Si dep
pre−SN
SN unmix
SN mix
time (dump)
log₁₀(mass fraction)

Fig. 5.— Evolution of and isotope distribution in $25\,\mathrm{M}_\odot$ stars of L03 abundances. *Left Column:* Standard values of the helium burning reaction rates, $(R_{3\alpha}, R_{\alpha,12}) = (1.0, 1.2)$. *Right Column:* $R_{3\alpha}$ enhanced by $18\,\%$: $(R_{3\alpha}, R_{\alpha,12}) = (1.18, 1.2)$. **Top Row:** Convective history as a function of time until core collapse. The ordinate is the mass coordinate from the center of the star. The green hatched areas are fully convective, and the red cross hatched areas are semiconvective. The blue and purple shading indicate net energy generation from burning and neutrino losses, with blue positive and purple negative. For more details see Woosley et al. (2002). The vertical lines show the snapshots we use and are explained in more detail in the test. **Middle Row:** Stellar structure at the pre-supernova stage as a function of the enclosed mass (truncated at $10\,\mathrm{M}_\odot$). *Dark gray* indicates the neutronized regions in which nucleosynthesis was no longer followed. The *vertical black line* shows the final mass cut of the SN. The *light gray* indicates convective regions. The *solid gray line* shows the nuclear energy generation and the *dashed gray line* shows the density. **Bottom Row:** Distribution of isotopes inside the star as a function of mass coordinate for different evolution stages (y-axis, time increased downward). *Gray shading* indicates neutronized regions (until pre-SN) or location of the SN piston (SN lines) in which nucleosynthesis was no longer followed as those regions become part of the remnant. The *solid black line* shows the final mass cut of the SN. For the two stars shown here there was no fallback, so the mass cut and the piston mass coincide; this is not the case in general.

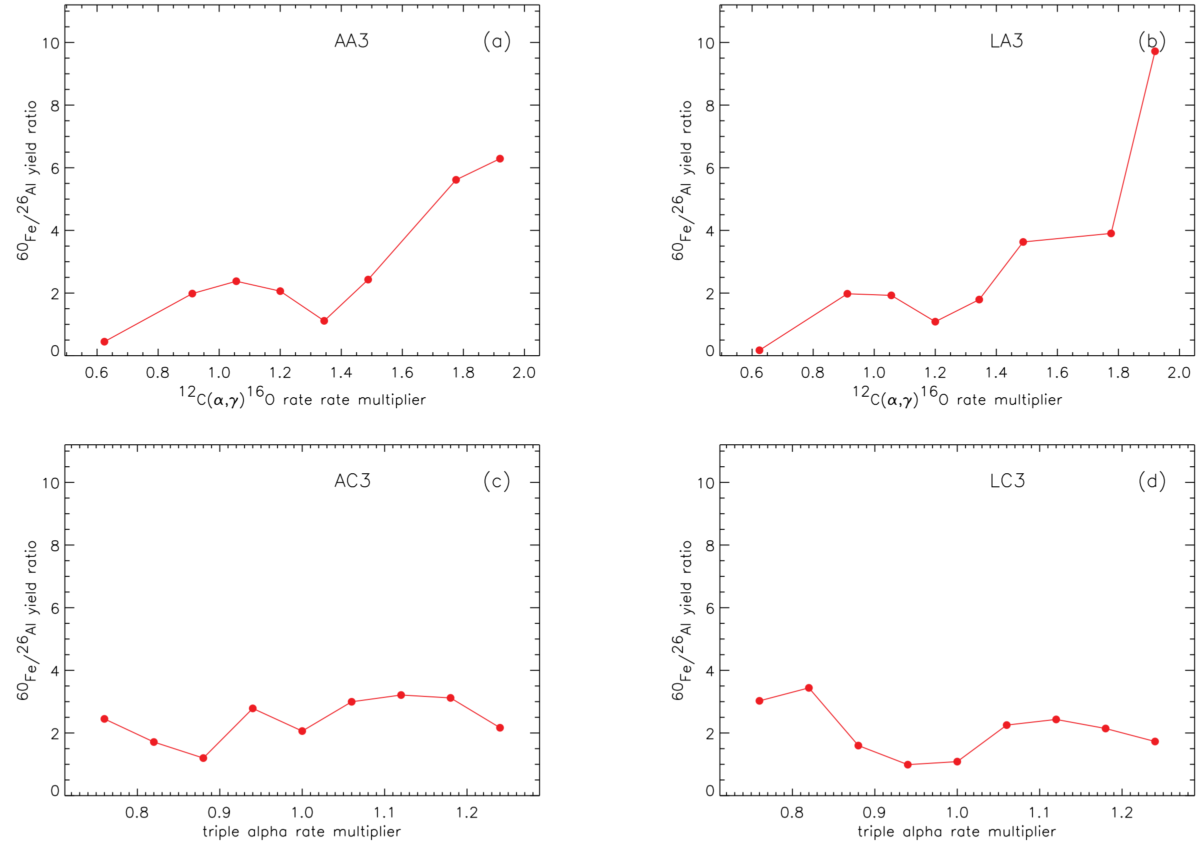

Fig. 6.— Mass ratio of yields of ^{60}Fe and ^{26}Al versus reaction rate, averaged over three stars ($15\,M_\odot$, $20\,M_\odot$, and $25\,M_\odot$). For details see the text. **(a)** AA series. **(b)** LA series. **(c)** AC series. **(d)** LC series.